Experimental Results for H2 Formation from H and H and Implications for First Star Formation

H. Kreckel, *et al.*

Science **329**, 69 (2010);
DOI: 10.1126/science.1187191

3. L. D. Jacobson, C. F. Williams, J. M. Herbert, *J. Chem. Phys.* **130**, 124115 (2009).
4. A. L. Sobolewski, W. Domcke, *Phys. Chem. Chem. Phys.* **4**, 4 (2002).
5. L. Kevan, *Acc. Chem. Res.* **14**, 138 (1981).
6. J. Schnitker, P. J. Rossky, *J. Chem. Phys.* **131**, 037102 (2009).
7. Y. Kimura, J. C. Alfano, P. K. Walhout, P. F. Barbara, *J. Phys. Chem.* **98**, 3450 (1994).
8. M. S. Pshenichnikov, A. Baltuska, D. A. Wiersma, *Chem. Phys. Lett.* **389**, 171 (2004).
9. A. E. Bragg, J. R. R. Verlet, A. Kammrath, O. Cheshnovsky, D. M. Neumark, *Science* **306**, 669 (2004).
10. B. J. Schwartz, P. J. Rossky, *J. Chem. Phys.* **101**, 6902 (1994).
11. K. Yokoyama, C. Silva, D. H. Son, P. K. Walhout, P. F. Barbara, *J. Phys. Chem. A* **102**, 6957 (1998).
12. B. J. Schwartz, P. J. Rossky, *Phys. Rev. Lett.* **72**, 3282 (1994).
13. B. J. Schwartz, P. J. Rossky, *J. Chem. Phys.* **101**, 6917 (1994).
14. A. Baltuska, M. F. Emde, M. Pshenichnikov, D. A. Wiersma, *J. Phys. Chem. A* **103**, 10065 (1999).
15. M. C. Cavanagh, I. Martini, B. J. Schwartz, *Chem. Phys. Lett.* **396**, 359 (2004).
16. C. J. Smallwood, R. E. Larsen, W. J. Glover, B. J. Schwartz, *J. Chem. Phys.* **125**, 074102 (2006).
17. R. E. Larsen, W. J. Glover, B. J. Schwartz, *J. Chem. Phys.* **131**, 037101, author reply 037102 (2009).
18. Materials and methods are available as supporting material on *Science* Online.
19. T. Sommerfeld, A. DeFusco, K. D. Jordan, *J. Phys. Chem. A* **112**, 11021 (2008).
20. R. E. Larsen, M. J. Bedard-Hearn, B. J. Schwartz, *J. Phys. Chem. B* **110**, 20055 (2006).
21. D. M. Bartels, K. Takahashi, J. A. Cline, T. W. Marin, C. D. Jonah, *J. Phys. Chem. A* **109**, 1299 (2005).
22. L. Turi, G. Hantal, P. J. Rossky, D. Borgis, *J. Chem. Phys.* **131**, 024119 (2009).
23. T. W. Kee, D. H. Son, P. Kambhampati, P. F. Barbara, *J. Phys. Chem. A* **105**, 8434 (2001).
24. J. Schnitker, K. Motakabbir, P. J. Rossky, R. A. Friesner, *Phys. Rev. Lett.* **60**, 456 (1988).
25. M. J. Tauber, R. A. Mathies, *J. Phys. Chem. A* **105**, 10952 (2001).
26. S. J. Rosenthal, B. J. Schwartz, P. J. Rossky, *Chem. Phys. Lett.* **229**, 443 (1994).
27. M. J. Tauber, R. A. Mathies, *J. Am. Chem. Soc.* **125**, 1394 (2003).
28. G. E. Walrafen, *J. Soln. Chem.* **2**, 159 (1973).
29. M. Boero, M. Parrinello, K. Terakura, T. Ikeshoji, C. C. Liew, *Phys. Rev. Lett.* **90**, 226403 (2003).
30. F.-Y. Jou, G. R. Freeman, *J. Phys. Chem.* **83**, 2383 (1979).

31. This research was funded by NSF under grant CHE-0908548. We thank M. C. Larsen and A. E. Bragg for helpful discussions, C. N. Mejia for performing the preliminary Hartree-Fock calculations that we used to generate the new electron-water pseudopotential, and K. D. Jordan for a critical reading of the manuscript.

Supporting Online Material

www.sciencemag.org/cgi/content/full/329/5987/65/DC1
Materials and Methods
SOM Text
Figs. S1 to S4
Table S1
References

15 March 2010; accepted 14 May 2010
10.1126/science.1189588

Experimental Results for H_2 Formation from H^- and H and Implications for First Star Formation

H. Kreckel,[1]*† H. Bruhns,[1]‡ M. Čížek,[2] S. C. O. Glover,[3] K. A. Miller,[1] X. Urbain,[4] D. W. Savin[1]

During the epoch of first star formation, molecular hydrogen (H_2) generated via associative detachment (AD) of H^- and H is believed to have been the main coolant of primordial gas for temperatures below 10^4 kelvin. The uncertainty in the cross section for this reaction has limited our understanding of protogalaxy formation during this epoch and of the characteristic masses and cooling times for the first stars. We report precise energy-resolved measurements of the AD reaction, made with the use of a specially constructed merged-beams apparatus. Our results agreed well with the most recent theoretically calculated cross section, which we then used in cosmological simulations to demonstrate how the reduced AD uncertainty improves constraints of the predicted masses for Population III stars.

More than 40 years ago, Saslaw and Zipoy (*1*) proposed that the formation of neutral molecular hydrogen played a central role in the cooling of primordial gas. Collisions of atomic H with molecular H_2 transfer kinetic energy from the H into internal energy of the H_2 through ro-vibrational excitation of the molecule. Subsequently, the molecule can radiatively relax and the emitted photon may escape from the cloud, thereby cooling the gas. Recent numerical models for the formation of the first (Population III) stars have demonstrated the importance of primordial H_2 as a coolant (*2*–*4*).

During the epoch of first star formation, H_2 was formed primarily via the associative detachment (AD) reaction (*3*),

$$H^- + H \rightarrow H_2^- \rightarrow H_2 + e^- \qquad (1)$$

Although this is the simplest anion-neutral chemical reaction, theory and experiment have failed to reach consensus for both the magnitude and energy dependence of the rate coefficient (*5*). This uncertainty severely limits our ability to model protogalaxies and metal-free stars forming from initially ionized gas, such as in H II regions created by earlier Population III stars (*5*, *6*). For example, it limits our ability to predict whether a given protogalactic halo can cool and condense on a sufficiently short time scale before it is gravitationally disrupted through a collision with another protogalactic halo (*5*). Additionally, the cosmological simulations we have performed for this work show that for gas in free fall, the resulting spread in the minimum gas temperature—and in the gas density at which this minimum is reached—leads to a factor of >20 difference in the Jeans mass. Finally, for shocked gas undergoing isobaric collapse, the time required to reach the cosmic microwave background temperature can differ by up to a factor of 3. This affects the likelihood that such gas will cool and collapse to form a star before undergoing another shock (*6*).

The three most recent theoretical calculations for Eq. 1 have not converged, although they all used the same potential for the intermediate H_2^- anion. The results of Sakimoto (*7*) and Čížek *et al*. (*8*) are in good agreement with one another but not with the calculations of Launay *et al*. (*9*). The room-temperature flowing afterglow results of (*10*–*12*), however, are discrepant with the calculations of Sakimoto and Čížek *et al*. but are in reasonable agreement with those of Launay *et al*. See (*13*) for a brief review. Unfortunately, the existing experimental work provides no constraint on the temperature dependence for Eq. 1, which limits the ability of these measurements to benchmark theory. Considering all these issues, we have designed and built a dedicated merged-beams apparatus in order to perform energy-resolved AD measurements spanning the entire relevant collision energy range.

An overview of the experiment is shown in Fig. 1; a detailed description is given in (*14*). In the first leg of the apparatus, we extract an H^- beam from a negatively biased ion source to achieve a beam energy eU_s of ~10 keV. We collimate it via standard ion beam technology. The atomic H beam is generated in the central portion of the second leg of the apparatus, where ~7.4% of the H^- is neutralized by photodetachment (PD) with a laser diode array at 975 nm with continuous-wave power of 1.4 kW. At the photon energy (1.25 eV) and power density used, the PD process produces exclusively ground-state H atoms. The PD occurs in the center of a drift tube, 1.2 m in length, used to control the relative energy between the H^- and H beams. When a voltage $-U_f$ is applied to the tube, the H^- ions are decelerated as they enter the tube and are then accelerated

[1]Columbia Astrophysics Laboratory, Columbia University, New York, NY 10027, USA. [2]Charles University Prague, Faculty of Mathematics and Physics, Institute of Theoretical Physics, 180 00 Praha 8, Czech Republic. [3]Zentrum für Astronomie der Universität Heidelberg, Institut für Theoretische Astrophysik, 69120 Heidelberg, Germany. [4]Institute of Condensed Matter and Nanosciences, Université Catholique de Louvain, Louvain-la-Neuve B-1348, Belgium.

*Present address: Department of Chemistry, University of Illinois, Urbana, IL 61801, USA.
†To whom correspondence should be addressed. E-mail: hkreckel@illinois.edu
‡Present address: INFICON GmbH, D-50968 Cologne, Germany.

back to their initial energy upon leaving. The neutral H atoms are created at an energy of $E_H = e(U_s - U_f)$ and maintain this energy after leaving the drift tube. Voltages of $-281\ V \leq -U_f \leq -1\ V$ were used, corresponding to center-of-mass collision energies E_{cm} from 3.7 meV to 1 eV. The lower end of the E_{cm} scale is limited by the angular spread of the merged beams (fig. S2), which are confined by two circular apertures before and after the PD region (5 mm in diameter, 2.8 m apart).

The interaction region begins with an electrostatic plate used to chop the H^- beam. The neutral beam is chopped by switching the laser. By chopping both beams out of phase with one another, the signal from H_2 generated in the interaction region can be extracted from the various backgrounds (*14*, *15*). Two rotating-wire beam profile monitors are used to record the ion and neutral beam profiles needed to determine the merged-beams overlap form factor Ω (*16*, *17*). The interaction region ends with an electrostatic quadrupole, which deflects the H^- ions into a Faraday cup used to continuously record the current. The neutral H particle current I_H (measured in amperes) in the interaction region is determined by calibrating the secondary electron emission of a neutral cup situated at the end of the beamline.

In the interaction region, the AD process creates ~100 s^{-1} of H_2 with a kinetic energy of 20 keV. The source potential is varied with U_f so that the sum of the parent H^- and H energies is 20 keV for all values of U_f (*14*). The H_2 is filtered from the ~10 keV stream of ~4×10^{11} s^{-1} H atoms in two steps. First, the H_2 and H are sent through a differentially pumped gas cell (length ~80 cm) with a He pressure of 2×10^{-4} torr. In the gas cell, electron stripping converts ~5% of the H_2 into H_2^+. The stripping cross section for 20 keV H_2 in helium is $\sigma_{st} = 1.04 \times 10^{-16}$ cm^2 with an uncertainty of 16.5% (*18*). This constitutes the largest contribution to the uncertainty of our absolute scale. Experimental studies for stripping of room-temperature and ro-vibrationally excited H_2 on He and H_2 indicate that the unknown ro-vibrational distribution of the H_2 generated by the AD process introduces an additional 10% uncertainty (*13*, *19*, *20*).

The He column density (N_{He}) in the gas cell is determined by measuring the H^- loss from a traversing beam due to single and double electron detachment. The cross sections for these processes are well known (*21*, *22*), allowing us to calibrate N_{He} to within 9% accuracy.

At the exit of the gas cell, two sequential electrostatic cylindrical energy analyzers select out the 20 keV H_2^+ ions and direct them onto a channel electron multiplier (CEM) with near-unity detection efficiency (*23*). After background subtraction, typical CEM signal rates S on the order of a few hertz are observed.

In our experiments, we measured the product of the AD cross section σ_{ad} and the relative velocity v_r convolved with the experimental velocity spread. The spread was calculated from geometric models of the overlapping beams, which showed excellent agreement with the beam shapes measured at the beam profile monitors. The measured rate coefficient is

$$\alpha = \langle \sigma_{ad} v_r \rangle = \frac{S}{\sigma_{st} N_{He}} \frac{e^2 v_{H^-} v_H}{I_{H^-} I_H} \frac{1}{\Omega} \quad (2)$$

where v_{H^-} and v_H are the velocities of the H^- and H beams, respectively, and the angle brackets denote the average over the velocity spread of the experiment. In Fig. 2, our experimental results are compared to the calculations of Čížek *et al.* (*8*). The agreement between experiment and theory in both magnitude and energy dependence is strong.

We have used the results of Čížek *et al.* to generate a thermal rate coefficient assuming a Maxwell-Boltzmann energy distribution. In (*8*) the cross section for Eq. 1 between 10^{-3} and 1 eV was calculated using a nonlocal resonance model in which the short-lived $H_2^{-2}\Sigma_u^+$ collision complex interacts with the H_2 $X^1\Sigma_g^+ + e^-$ continuum. To determine rate coefficients from 1 to 10^4 K, it was necessary for us to extend that work at lower energies (10^{-6} to 10^{-3} eV) and also at higher energies (1 to 10 eV), where almost 100 partial waves had to be included. The $H_2^{-2}\Sigma_g^+$ state was not taken into account because the repulsive character of this state suggests that the cross sections will be much smaller than contributions from the $H_2^{-2}\Sigma_u^+$ state. To simplify the implementation of our experimentally confirmed thermal rate coefficient into cosmological models, we provide an analytical fit function in table S1.

In gas that is cooling and recombining from an initially ionized state—for example, in an H II region surrounding a previous Population III star—H_2 forms efficiently via the AD reaction owing to the high abundance of free electrons. At times much greater than the first few recombination times, the H_2 fraction tends toward an almost constant value (*24*) that depends critically on the AD rate coefficient.

To examine the effect of our thermal AD rate coefficient on primordial star formation, we performed a set of high-resolution simulations of primordial gas evolving within an initially ionized protogalactic halo. The simulation is intended to represent a low-mass protogalaxy forming in a relic H II region. We represent the dark matter halo with a fixed background potential, assuming a Navarro-Frenk-White density profile (*25*) and a total dark matter mass of 9.7×10^5 solar masses ($M_\odot$). The associated gas mass of 2×10^5 $M_\odot$ has a starting temperature of 10^4 K and is initially in hydrostatic equilibrium. We simulate the evolution of the gas with a modified version of the GADGET 2 smoothed particle hydrodynamics (SPH) code (*26*) and represent the 2×10^5 $M_\odot$ of gas with 2 million SPH particles, giving us a particle mass of 0.1 $M_\odot$ and a minimum mass resolution of 10 $M_\odot$ (*13*).

Figure 3 compares the state of the gas for five different runs at the end of the simulations. Each point corresponds to a spherical shell of material centered about the cloud center (*13*). Runs 1 and 2 used the previous upper and lower limits for the rate coefficient of Eq. 1 from (*5*), respectively; run 3 used our new thermal rate coefficient, whereas runs 4 and 5 used values that were 25% larger or smaller than this, respectively, representing the remaining systematic uncertainty in the rate coefficient. The temperature for each run is plotted in Fig. 3A. In run 1, the high AD rate leads to a higher asymptotic H_2 abundance (Fig. 3B), and hence a higher HD abundance

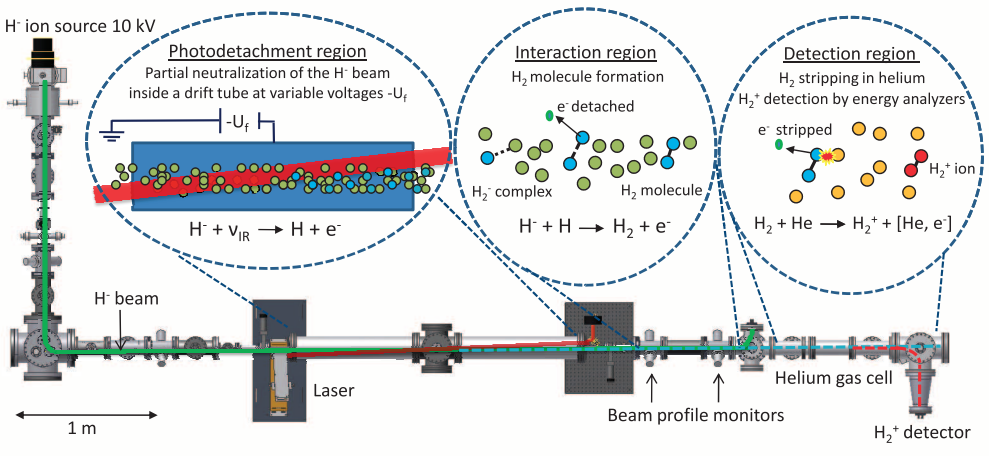

Fig. 1. Schematic of the merged-beams apparatus used to measure the H_2 associative detachment reaction. Infrared laser photons are denoted by ν_{IR}.

(Fig. 3C), as HD is rapidly produced from H_2 by the reaction

$$H_2 + D^+ \rightarrow HD + H^+ \quad (3)$$

In this run, the HD abundance becomes large enough to dominate the cooling. Because the critical density of HD—the density at which its rotational level populations approach their local thermodynamic equilibrium values—is much higher than that of H_2, and because HD can cool the gas to much lower temperatures, the gas remains cold up to hydrogen nuclei number density $n \approx 10^6$ cm^{-3}.

In run 2, the lower AD rate leads to a lower asymptotic H_2 abundance, and in this case the amount of HD that forms is never sufficient to dominate the cooling. Therefore, the gas reaches a minimum temperature $T_{min} \approx 200$ K at a density close to the H_2 critical density, and thereafter begins to heat up.

This difference in behavior has important consequences for the characteristic mass of the Population III stars that are formed, which is closely related to the Jeans mass of the gas at the density of minimum temperature (*27*). The Jeans mass is smaller in run 1 than in run 2 by a factor of >20, demonstrating that the previous uncertainty in the AD rate coefficient results in a very large uncertainty in the predicted mass of the Population III stars.

The results for runs 3 to 5 show that the measurements reported here explicitly constrain the situation. Runs 3 and 5 produce almost identical results, and although in run 4 slightly more HD is created and lower temperatures are reached, the qualitative evolution is the same as in the other runs. HD cooling never becomes dominant, and the uncertainty in the characteristic Population III mass is reduced from a factor of >20 to a factor of ~2.

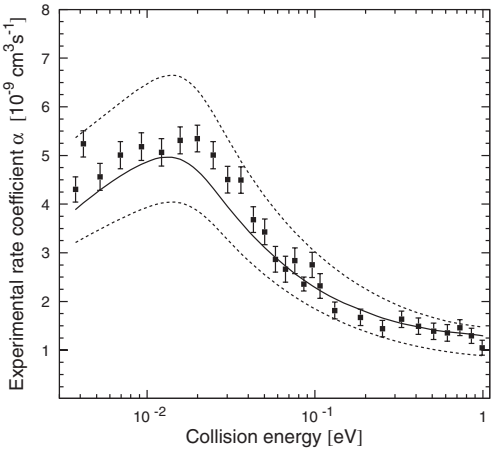

Fig. 2. Experimental rate coefficient $\alpha = \langle \sigma_{ad} v_r \rangle$ for Eq. 1. The error bars show the 1σ statistical uncertainty of the measurement (*13*). The dashed error bands present the systematic experimental uncertainty of 25% (at an estimated 1σ level). The solid line depicts the theoretical results reported in (*8*) multiplied by v_r and convolved with the experimental velocity distribution, which is non-Maxwellian for collision energies above ~0.01 eV. See fig. S3 for a plot of the thermal rate coefficient derived from the theoretical cross-section results. An analytical fit for the thermal rate coefficient is shown in table S1.

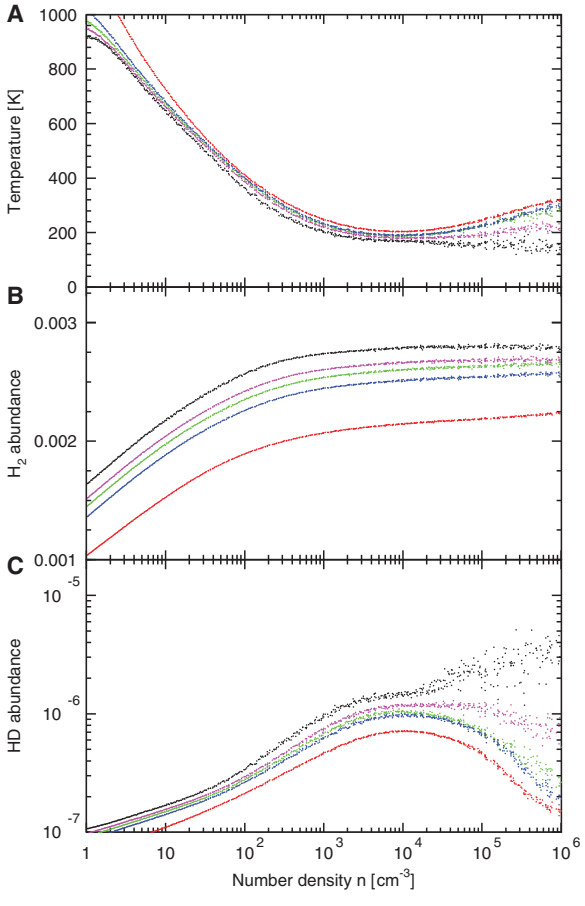

Fig. 3. (**A** to **C**) Simulations of primordial gas evolving in an initially ionized protogalactic halo, using different AD rate coefficients. Results are shown for (A) absolute temperature, (B) H_2 abundance, and (C) HD abundance. The black and red dots mark runs 1 and 2, representing the previous upper and lower limits for the AD rate coefficient, respectively. Run 3 (green) shows the results using our new thermal rate coefficient. For run 4 (magenta), a rate coefficient 25% greater than this was used, representing the remaining uncertainty in the AD rate; for run 5 (blue), a rate coefficient 25% smaller was used. The models were run at a redshift $z \approx 25$ where the cosmic microwave background temperature was $T_{CMB} \approx 70$ K.

References and Notes

1. W. C. Saslaw, D. Zipoy, *Nature* **216**, 976 (1967).
2. T. Abel, G. L. Bryan, M. L. Norman, *Science* **295**, 93 (2002); published online 15 November 2001 (10.1126/science.1063991).
3. V. Bromm, N. Yoshida, L. Hernquist, C. F. McKee, *Nature* **459**, 49 (2009).
4. N. Yoshida, K. Omukai, L. Hernquist, *Science* **321**, 669 (2008).
5. S. C. Glover, D. W. Savin, A.-K. Jappsen, *Astrophys. J.* **640**, 553 (2006).
6. S. C. O. Glover, T. Abel, *Mon. Not. R. Astron. Soc.* **388**, 1627 (2008).
7. K. Sakimoto, *Chem. Phys. Lett.* **164**, 294 (1989).
8. M. Čížek, J. Horáček, W. Domcke, *J. Phys. B* **31**, 2571 (1998).
9. J. M. Launay, M. Le Dourneuf, C. J. Zeippen, *Astron. Astrophys.* **252**, 842 (1991).
10. A. L. Schmeltekopf, F. C. Fehsenfeld, E. E. Ferguson, *Astrophys. J.* **148**, L155 (1967).
11. F. C. Fehsenfeld, C. J. Howard, E. E. Ferguson, *J. Chem. Phys.* **58**, 5841 (1973).
12. O. Martinez Jr., Z. Yang, N. B. Betts, T. P. Snow, V. M. Bierbaum, *Astrophys. J.* **705**, L172 (2009).
13. See supporting material on *Science* Online.
14. H. Bruhns *et al.*, *Rev. Sci. Instrum.* **81**, 013112 (2010).
15. C. C. Havener, M. S. Huq, H. F. Krause, P. A. Schulz, R. A. Phaneuf, *Phys. Rev. A* **39**, 1725 (1989).
16. R. A. Phaneuf, C. C. Havener, G. H. Dunn, A. Müller, *Rep. Prog. Phys.* **62**, 1143 (1999).
17. D. G. Seely *et al.*, *Nucl. Instrum. Methods A* **585**, 69 (2008).
18. R. Browning, C. J. Latimer, H. B. Gilbody, *J. Phys. B* **3**, 667 (1970).
19. A. Bouliou, M. Sarret, P. Frere, *C. R. Acad. Sci. Paris* **296II**, 1377 (1983).
20. I. D. Williams, J. Geddes, H. B. Gilbody, *J. Phys. B* **17**, 811 (1984).
21. T. J. Kvale, J. S. Allen, X. D. Fang, A. Sen, R. Matulioniene, *Phys. Rev. A* **51**, 1351 (1995).
22. C. F. Barnett, Ed., *Atomic Data for Fusion. Volume 1: Collisions of H, H_2, He, and Li Atoms and Ions with Atoms and Molecules* (Controlled Fusion and Atomic Data Center, Oak Ridge National Laboratory, ORNL-6086, 1990).
23. D. H. Crandall, J. A. Ray, C. Cisneros, *Rev. Sci. Instrum.* **46**, 562 (1975).
24. M. Tegmark *et al.*, *Astrophys. J.* **474**, 1 (1997).
25. J. F. Navarro, C. S. Frenk, S. D. M. White, *Astrophys. J.* **490**, 493 (1997).
26. V. Springel, *Mon. Not. R. Astron. Soc.* **364**, 1105 (2005).
27. V. Bromm, P. F. Coppi, R. B. Larson, *Astrophys. J.* **564**, 23 (2002).

28. Supported by the Deutscher Akademischer Austauschdienst (H.B.); Grantová Agentura České Republiky grant 202/07/0833 and "Výzkumný zámer" grant MSM 0021620860 (M.Č.); German Bundesministerium für Bildung und Forschung (via STAR FORMAT grant 05A09VHA), Deutsche Forschungsgemeinschaft grant KL 1358/4, and Heidelberg University, sponsored by the German Excellence Initiative and the Landesstiftung Baden-Württemberg (International Collaboration II grant P-LS-SPII/18) (S.C.O.G.); and NSF grants CHE-0520660, AST-0606960, and AST-0807436. X.U. is a Senior Research Associate of the Fonds de la Recherche Scientifique–FNRS, Belgium.

Supporting Online Material

www.sciencemag.org/cgi/content/full/329/5987/69/DC1
Materials and Methods
Figs. S1 to S3
Table S1
References

18 January 2010; accepted 12 May 2010
10.1126/science.1187191